CHEMISTRY OF MATERIALS

Article

pubs.acs.org/cm

High-Performance *n*-Type Organic Transistor with a Solution-Processed and Exfoliation-Transferred Two-Dimensional Crystalline Layered Film

Sang Kyu Park,[†] Jong H. Kim,[†] Seong-Jun Yoon,[†] Oh Kyu Kwon,[†] Byeong-Kwan An,[‡] and Soo Young Park*,[†]

[†]Creative Research Initiative Center for Supramolecular Optoelectronic Materials and WCU Hybrid Materials Program, Department of Materials Science and Engineering, Seoul National University, ENG 445, Seoul, 151-744, Korea

[‡]Department of Chemistry, The Catholic University of Korea, Bucheon-si, Geyonggi-do 420-753, Korea

Supporting Information

ABSTRACT: High-performance *n*-type organic field-effect transistors (OFETs) based on 2-dimensional (2D) crystalline layered films of the novel dicyanodistyrylbenzene (DCS) derivative (2*Z*,2′*Z*)-3,3′-(1,4-phenylene)bis(2-(3,5-bis(trifluoromethyl)phenyl)-acrylonitrile) (CN-TFPA) were fabricated using a simple solution process. The OFETs showed electron mobilities of up to 0.55 $cm^2\ V^{-1}\ s^{-1}$, which was attributed to the appropriate electron affinity and dense molecular packing in the well-ordered 2D terrace structure. Because of the easy exfoliation capabilities of the CN-TFPA 2D crystalline layers, 2−10 CN-TFPA molecular monolayers could be successfully transferred onto the substrates, enabling the fabrication of ultrathin OFET devices with an active layer thickness of ∼30 nm.

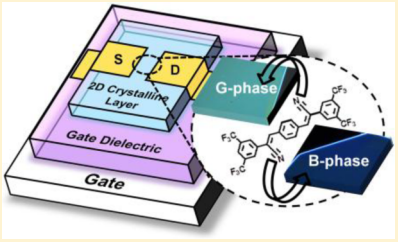

KEYWORDS: *single-crystalline organic field-effect transistor, n-type semiconductor, two-dimensional single-crystal, solution-process, mechanical cleavage*

INTRODUCTION

In recent years, single-crystalline organic semiconductors have been intensively studied as a promising alternative to amorphous silicon-based materials in a wide range of electronic applications, especially organic field-effect transistors (OFETs).[1] Single-crystalline organic semiconductors are particularly suited to OFETs because of characteristics such as their high carrier mobility, which derives from the lack of grain boundaries and the minimal number of charge trap sites, and their merits in terms of ease of processing and deposition on flexible substrates. In addition, the solution-processed self-assembly of organic semiconductors offers opportunities for the low-cost and large-area processing of next-generation electronics. Simple solution-processed single-crystalline OFETs (SC-OFETs) have therefore attracted much interest;[2] to date, a variety of high-performance *p*-type SC-OFETs fabricated via various solution processes have been successfully demonstrated, and some of them have shown performances far superior to that of amorphous silicon.[3]

In contrast with solution-processed *p*-type SC-OFETs, however, it remains a challenge to fabricate solution-processed *n*-type SC-OFETs, because the building blocks for high-performance *n*-type SC-OFETs inherently have much more complicated molecular design prerequisites; specifically, they should show not only dense molecular packing and good solubility, but also high electron affinity (or low lowest unoccupied molecular orbitals (LUMOs)) for an efficient electron injection from electrodes. In particular, the electron-withdrawing groups essential for the lowering of the LUMO level in *n*-type building blocks may destroy the highly crystalline structure or decrease the degree of molecular ordering, owing to their bulkiness and the presence of electrostatic forces. As a result, only a limited number of *n*-type π-conjugated systems have been introduced so far; these include perylenediimide,[4] naphthalenediimide,[5] and oligothiophene.[6] Very recently, π-conjugated dicyanodistyrylbenzene (DCS)-type derivatives with electron-withdrawing trifluoromethyl (−CF3) units have also proven their promising application potential toward high-performance *n*-type OFETs, because of their unique structural features.[7−9] The "twist elasticity" behavior of the DCS backbone, which exhibits large torsional changes in the π-conjugated backbone from the isolated solution state to the aggregated solid state, played an important role in achieving a coplanar structure, leading to close π−π contacts in the self-assembled condensed state.[10] In addition, the electron-withdrawing −CN and −CF3 groups not only decreased the LUMO to a suitable level, but also stabilized the laterally adjacent molecules by building up specific noncovalent intermolecular interactions, which led to tight and dense molecular packing.[11]

In the course of the continuous systematic syntheses of the DCS-backbone building blocks for the *n*-type SC-OFET

Received: June 7, 2012
Revised: August 1, 2012
Published: August 1, 2012

dx.doi.org/10.1021/cm301775c | *Chem. Mater.* 2012, 24, 3263−3268

materials, we found that one of our newly synthesized DCS derivatives, (2Z,2′Z)-3,3′-(1,4-phenylene)bis(2-(3,5-bis(trifluoromethyl)phenyl)acrylonitrile) (CN-TFPA) (Scheme 1), possessed a strong tendency to form well-ordered two-

Scheme 1. Synthetic Procedure to Obtain CN-TFPA

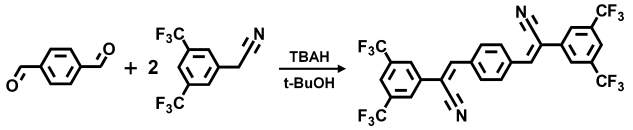

dimensional (2D) crystals in large areas directly on the substrate, via a simple solution-processed self-assembly process. In this Article, we report that the 2D crystalline layer structure of CN-TFPA, which is conceived as a new, advantageous feature of the DCS π-conjugated system to build up high *n*-type conducting channels, can serve as an effective scaffold for the fabrication of solution-processed, high-performance, ultrathin *n*-type SC-OFETs; this is due to its dense molecular packing, low LUMO levels, and the fact that it can be easily exfoliated to give thin-layered molecular assembly sheets.

EXPERIMENTAL SECTION

Materials. CN-TFPA was synthesized via Knoevenagel condensation between 2-(3,5-bis(trifluoromethyl)phenyl)acetonitrile and terephthalaldehyde, as shown in Scheme 1. All chemicals were purchased commercially and used without further purification. Terephthalaldehyde (0.8 g) and 2-(3,5-bis(trifluoromethyl)phenyl)acetonitrile (3.0 g) were dissolved in 50 mL of *t*-butyl alcohol. A 0.84 mL aliquot of tetrabutylammonium hydroxide was slowly dropped into the solution, using a reaction temperature of 50° and a reaction time of 2 h. The precipitated product, (2Z,2′Z)-3,3′-(1,4-phenylene)bis(2-(3,5-bis(trifluoromethyl)phenyl)acrylonitrile), was then filtered and purified by flash column chromatography with dichloromethane. For further purification, the product was recrystallized in a dichloromethane/methanol solution. Finally, sublimation purification was conducted under high vacuum (below 1×10^{-6} Torr), and a bright greenish-yellow powder was obtained as the product. The chemical structure of CN-TFPA was confirmed using ^{1}H NMR, ^{13}C NMR, elemental analysis (EA), and mass spectroscopy (vide infra).

^{1}H NMR (300 MHz, $CDCl_3$) δ [ppm]: 8.13 (s, 4H, Ar−H), 8.10 (s, 4H, Ar−H), 7.95 (s, 2H, Ar−H), 7.69 (s, 2H, vinyl-H). ^{13}C NMR (500 MHz, $CDCl_3$) δ [ppm]: 143.70, 136.55, 135.58, 133.60, 133.33, 133.06, 132.79, 130.55, 126.42, 124.20, 123.46, 122.02, 116.81, 111.23. MS (FAB) (*m*/*z*): Calculated for C28H12F12N2: 604.08, Found: 604.08. Anal. Calculated for C28H12F12N2: C, 55.64; H, 2.00; F, 37.72; N, 4.63. Found: C, 55.71; H, 1.98; N, 4.63.

Characterization. ^{1}H NMR was recorded using a Bruker, Avance-300 (300 MHz) instrument, in a $CDCl_3$ solution. ^{13}C NMR was recorded using a Bruker, Avance-500 (500 MHz) instrument, in a $CDCl_3$ solution. Elemental analysis was conducted on CN-TFPA using a CE Instruments, EA1110 elemental analyzer. The mass spectrum of CN-TFPA was measured using a JEOL, JMS-600W mass spectrometer. Out-of-plane X-ray diffraction measurements were performed using a D8-Advance X-ray diffractometer (Bruker Miller Co., Germany), and the operating conditions were a step size of 0.02, a scan rate of 3 degree/min, a 40 kV generator voltage, a 40 mA tube current, and room temperature (Cu std target λ = 1.5418 Å). Atomic force microscopy (AFM) was performed using a PSIA instrument XE-150 and a Bruker instrument multimode with a NanoScope V controller. AFM topographic and phase images were recorded simultaneously in either contact or noncontact mode. UV−visible absorption spectra were recorded on a Shimadzu, UV-1650 PC spectrometer. The photoluminescence (PL) spectra of each solid-state phase were measured using a Varian, Cary Eclipse, fluorescence spectrophotometer. Differential scanning calorimetry (DSC) was recorded using a Perkin-Elmer DSC7.

Sample Preparation. The nanoparticle suspension samples were prepared by typical simple precipitation method employing tetrahydrofuran and distilled water as solvent media. The CN-TFPA was dissolved in tetrahydrofuran with a concentration of 5×10^{-3} mol L^{-1}. Then distilled water was slowly injected in various volume fractions with total concentration of 5×10^{-6} mol L^{-1}. The suspensions were left for at least 2 h before absorption spectra measurements. The bulk single-crystals of CN-TFPA were obtained via a solvent diffusion crystal growth method using ethyl acetate/methanol.

Device Fabrication. To prepare the substrates, we rinsed the substrates with acetone and isopropyl alcohol for 10 min under ultrasonication. After rinsing, 10 min of UV (360 nm) O^3 treatment was applied.

For simple solution processable single crystalline field-effect transistor fabrication, we employed the solvent evaporation crystal growth technique. We leaned an SiO_2/Si wafer on the inner wall of a 20 mL vial containing a 0.05 wt % CN-TFPA solution (in dichloromethane), under ambient conditions, as depicted in Supporting Information, Figure S3. CN-TFPA single crystal films were spontaneously grown (directly and slowly) on the substrates, which resulted in firm contact between substrates and the crystal films.[12] The resulting crystals were found to have two different surface-induced solid-state packing structures (**G**-phase and **B**-phase, vide infra). After crystal formation, the substrates were annealed at 50 °C for 1 h, to eliminate any residual solvent. 50 nm-thick source-drain Au electrodes were thermally deposited directly onto the crystalline layers through the metal mask, to fabricate top-contact SC-OFETs (the deposition rate was 0.1−0.2 Å/s) (Supporting Information, Figure S4).

For thermally evaporated vacuum deposited poly crystalline FETs fabrication, we introduced an octadecyltrichlorosilane (ODTS) layer for reduced charge trap sites as well as for domain enlargement. ODTS was treated in vapor phase in a vacuum oven; then the substrates were brought into nitrogen filled glovebox. Thirty nm thick CN-TFPA active layers were thermally deposited with deposition rate of 0.1−0.2 Å s^{-1} and different substrate temperatures (T_{SUB}) (RT, 50, and 70 °C), under a vacuum of 7×10^{-7} Torr.

To fabricate the transfer-printed thin-crystal OFETs via a mechanical cleavage method, we prepared mother crystals of 2D crystalline layers for the **G**/**B**-phase, using the solvent evaporation crystal growth technique. Scotch tape (3M) was attached to the top of the 2D crystalline layers, and pressed gently using fingers. By detaching the Scotch tape, we could obtain exfoliated, flaky, thin crystals from the mother **G**/**B**-phase crystals. Finally, we pressed the Scotch tape with the thin crystals onto the other SiO_2/Si substrate, so that we could transfer the thin crystals by detaching the Scotch tape. All of these procedures were carried out under ambient conditions. Finally, we took the samples into the nitrogen-filled glovebox, and thermally evaporated the Au electrodes, as presented in the fabrication of SC-OFETs section.

Transistor Measurements. The I−V characteristics of all of the OFETs were measured in a nitrogen-filled glovebox, using a Keithley 4200 SCS instrument connected to a probe station. The mobility values and V_{th} were obtained from the transfer curve in the saturated regime. For the charge carrier mobility calculations, we checked the source-drain channel width and the length of the individual devices using an optical microscope.

RESULTS AND DISCUSSION

CN-TFPA was prepared in a one-step Knoevenagel condensation reaction (Scheme 1). Because of the unique twisting conformation and polar substituents of CN-TFPA, it showed good solubility in common organic solvents such as dichloromethane, chloroform, and 1,2-dichloroethane; this solubility was attained despite the absence of the long alkyl chains that are commonly used to achieve good solubility in the rigid π-conjugated system, but are inactive and undesirable for the

dx.doi.org/10.1021/cm301775c | *Chem. Mater.* 2012, 24, 3263−3268

tuning of the electronic properties. Upon slow solvent evaporation, CN-TFPA molecules in a 0.20 wt % 1,2-dichloroethane solution readily self-assembled into a large, single crystal with terraced surfaces (Figure 1a). The step-terrace morphology was observed using atomic force microscopy (AFM), and was found to have a step size of approximately 1.4 nm, as shown in Figure 1b. The crystal films showed strongly anisotropic characteristics, as indicated by the uniform extinction of the reflected light intensity when the crystal films were rotated ±45° to the crossed polarizers (Figure 1a inset).

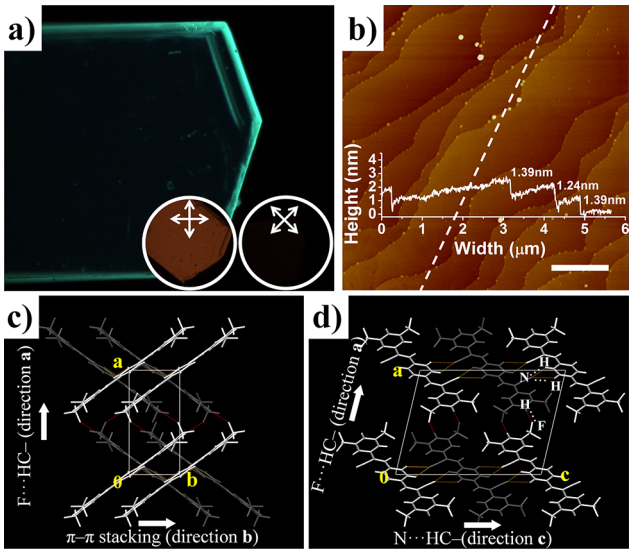

Figure 1. Fluorescent image of a single CN-TFPA crystal, taken using an optical microscope (circled image insets: birefringence image of same crystal using polarized optical microscope) (a). AFM image (scale bar: 1 μm) of a single CN-TFPA crystal (insets: thickness profile along dashed line) (b). Molecular stacking observed from single-crystal XRD analysis (the directions of the intermolecular interactions are illustrated using white arrows) (c, d).

To elucidate the 2D terrace structure of the CN-TFPA molecules in the single-crystal state, X-ray diffraction (XRD) analysis was performed on a single-crystal grown via solvent-diffusion crystal growth method. The molecular conformation and stacking structure of CN-TFPA are depicted in Figure 1c, d. It was clearly seen that the CN-TFPA had a quasi-planar molecular conformation in the condensed crystal state, although the twisted structure was more favored in the isolated state (see also Supporting Information, Figure S2), owing to its unique "twist elasticity" behavior. The quasi-planar CN-TFPA molecules bearing abundant electron-deficient groups were responsible for the strong π–π stacking interactions and the close interlayer distance of 3.09 Å along the ***b*** direction.[13] In addition, the continuously aligned H-bonding between the N of the cyano group and the two HC– of the laterally adjacent phenyl groups along direction ***c*** (8 different –N···HC– interactions (2.65, 2.72 Å) per molecule) (Figure 1d) played an essential role in producing the 2D crystal growth. The CN-TFPA molecules formed a layer-by-layer lamellar structure that was created via H-bonding between the F of the $-CF_3$ groups and the HC– of the adjacent phenyl groups along the direction ***a*** (4 different –F···HC– interactions (2.59 Å) per molecule), which was perpendicular to the plane ***bc***. However, the intermolecular H- bonding along the direction ***a*** (out-of-plane) is predicted to be much weaker than that along the direction ***c*** (in-plane), because of the smaller number of H-bonding sites (8 vs 4 for H-bonding along directions ***c*** and ***a***, respectively), and the intrinsically weak nature of the H-bonding between the F in the $-CF_3$ group and the phenyl HC–.[14] Consequently, this strong anisotropic intermolecular interaction between the plane ***bc*** and the direction ***a*** led to thin 2D lamellar CN-TFPA supramolecular structures with low-energy surfaced layers. It is worthy of note that both the –CN and $-CF_3$ units play a decisive role not only in achieving tight molecular packing and constructing a 2D layer structure via specific H-bonding, but also in efficiently stabilizing the LUMO level of CN-TFPA (HOMO: −6.98 eV, LUMO: −4.14 eV, bandgap: 2.84 eV, calculated from ultraviolet photoemission spectroscopy (UPS) and the optical band gap of vacuum deposited film, see Supporting Information, Figure S5a) via their electron-deficient characters; this stability is desirable for an efficient electron injection from the metal electrodes.

To form thin, large-area, well-ordered 2D crystalline layered CN-TFPA films for SC-OFET applications, we employed a simple "solvent evaporation crystal growth technique" (Supporting Information, Figure S3), in which the SiO_2/Si substrates were leaned on the inner wall of a 20 mL vial of 0.20–0.05 wt % CN-TFPA solution in 1,2-dichloroethane or tetrahydrofuran, during a slow solvent evaporation process in ambient conditions. Ultrauniform 2D CN-TFPA crystalline layer films with a thickness of 100–200 nm (approximately 60–130 layers) were grown directly on the substrate with *x*-*y* dimensions of a few millimeters; the films exhibited a green fluorescence emission (Figure 2a), similar to that shown in bulk single crystals of CN-TFPA. Interestingly, it was also found that blue fluorescent CN- TFPA crystalline films (Figure 2b) could be developed and isolated when dichloromethane or chloroform was used as a solvent medium; this was probably due to the different solvent properties, such as the polarity, boiling point, and vapor pressure.[15] The obtained blue fluorescent CN-

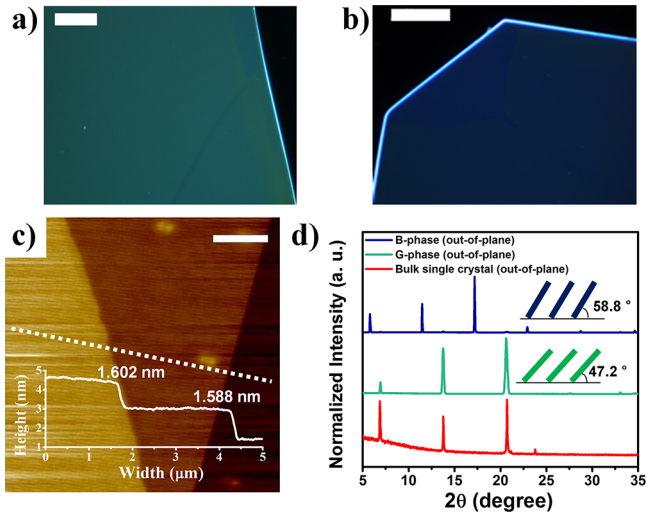

Figure 2. Fluorescent images of 2D crystalline CN-TFPA layers grown by solution evaporation crystal growth (scale bar: (a) 100 μm, (b) 50 μm). Molecular monolayer and bilayer from **B**-phase 2D sheet, measured using AFM (scale bar: 1 μm, inset: thickness profile along white dashed line) (c). Out-of-plane XRD analysis of the **B**-phase (blue line), **G**-phase (green line) and bulk single crystal (red line) (insets: schematic drawings of molecular stacks of each phase, with slipped angles to the plane ***bc***) (d).

dx.doi.org/10.1021/cm301775c | *Chem. Mater.* 2012, 24, 3263–3268

TFPA crystalline films also exhibited a neat step-terrace structure (Figure 2c) (hereinafter green and blue fluorescent CN-TFPA crystalline layers are denoted as **G**-phase and **B**-phase, respectively). In the out-of-plane XRD analysis of the **G**-phase and **B**-phase crystalline layers, these two layers were found to have a different slipped angle for the DCS π-conjugated backbone (Figure 2d). The plane of the DCS backbone in the **G**-phase was slipped with respect to the plane ***bc*** with a dihedral angle of about 47.2° (d_{100}: 1.37 nm), whereas that in the **B**-phase was more perpendicular to the plane ***bc***, with a dihedral angle of about 58.8° (d_{100}: 1.63 nm). In terms of carrier mobility, the **B**-phase was expected to be more efficient, since the π-electronic communication among neighboring molecules in the **B**-phase was better than that in the **G**-phase. By comparing out-of-plane X-ray diffraction peaks of bulk single-crystal with peaks of 2D crystalline layers (Figure 2d), we could assign that the **G**-phase 2D terrace structure have same packing motif with that of bulk single-crystal. Moreover, we could also observe coincidence between the PL spectra of bulk-crystals grown in solution and **G**-phase 2D terrace structure grown via solvent evaporation crystal growth technique because of the equivalent molecular packing states, as shown in Supporting Information, Figure S5b.

An investigation of the electrical performances of the **G**- and **B**-phase 2D layer films was carried out by fabricating top-contact SC-OFETs via the thermal deposition of Au electrodes through metal masks (details in Experimental Section). The SC-OFETs based on the **G**-phase 2D crystalline layer films showed typical *n*-type OFET behaviors, with electron mobility (μ_e) values as high as 0.03 $cm^2\ V^{-1}\ s^{-1}$, and an on/off current ratio of 10^4 (Figure 3a). As expected, however, μ_e was

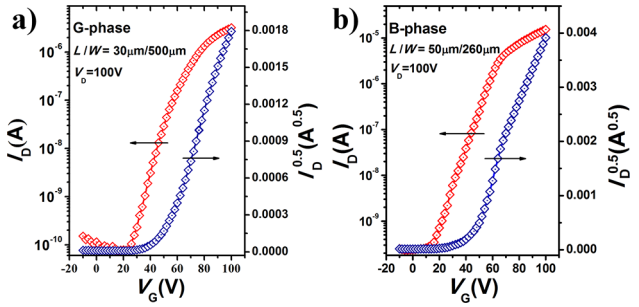

Figure 3. Measured *n*-type characteristics of the CN-TFPA crystal devices (a: **G**-phase, b: **B**-phase).

dramatically improved by more than 18 times in the **B**-phase SC-OFETs (μ_e = 0.55 $cm^2\ V^{-1}\ s^{-1}$), most likely because of the larger $\pi-\pi$ overlaps, which led to enhanced electronic communication (Figure 3b). For comparison, the poly crystalline FETs were also fabricated by vacuum thermal deposition, and a μ_e value as high as 0.34 $cm^2\ V^{-1}\ s^{-1}$ was obtained at T_{SUB} of 70 °C, which is still lower than that from **B**-phase 2D layered film-based SC-OFETs because of the large amount of grain boundaries and possible impurities in the poly crystalline state (see Supporting Information, Figure S6, 7 and Table 1 for detailed information). The 2D crystalline characteristics of the **B**-phase SC-OFETs were further confirmed in an anisotropic field-effect mobility study. Figure 4 shows that the anisotropic dependence of the mobility values was clearly observed when varying the measuring directions; the μ_e in the direction indicated by the large red arrow was approximately 2 times larger than that in the direction indicated

Table 1. Characterized Electrical Properties of CN-TFPA SC-OFETs

sample	μ_e [$cm^2\ V^{-1}\ s^{-1}$][a]	I_{on}/I_{off}	V_{th}[V][b]	n[c]
G-phase 2D layered films[d]	3.0×10^{-2} (1.1×10^{-2})	10^4	41	10
B-phase 2D layered films[d]	5.5×10^{-1} (4.6×10^{-1})	10^5	45	10
exfoliated **B**-phase 2D layered films[e]	5.3×10^{-2} (2.9×10^{-2})	10^4–10^5	38	5
vacuum deposited film (T_{SUB} = RT)[f]	5.9×10^{-2} (3.8×10^{-2})	10^6	44	9
vacuum deposited film (T_{SUB} = 50 °C)[f]	2.3×10^{-1} (1.8×10^{-1})	10^6	51	9
vacuum deposited film (T_{SUB} = 70 °C)[f]	3.4×10^{-1} (2.0×10^{-1})	10^6	50	9

[a]Maximum and average electron mobility value. [b]Average threshold voltage. [c]Number of devices tested. [d]Devices fabricated by solvent evaporation crystal growth technique. [e]Device fabricated by mechanical cleavage method. [f]Device fabricated by vacuum deposition technique with ODTS treated SiO_2/Si substrate.

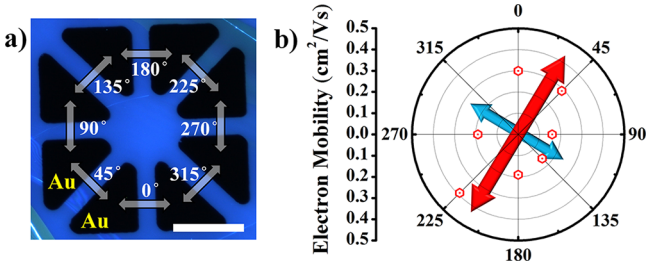

Figure 4. Schematic illustrating the measurement of the anisotropic field-effect mobility of the **B**-phase (scale bar: 200 μm) (a). Eight *n*-channel mobility values from the single crystalline **B**-phase 2D layer were measured every 45° (the value at 315° was not obtained) (red arrow in (b): speculated direction formed by the $\pi-\pi$ interaction) (b).

by the small blue arrow. The μ_e values in the directions indicated by the large red and small blue arrows were assumed to result from contributions from $\pi-\pi$ stacking and H-bonding (−CN···HC−), respectively. Importantly, the μ_e values along all directions exceeded 0.15 $cm^2\ V^{-1}\ s^{-1}$, indicating that the **B**-phase CN-TFPA SC-OFETs are very promising for practical OFET applications.

Besides the dense and tight molecular packing derived from the high-quality 2D crystals, the self-assembled CN-TFPA molecules possessed additional unique 2D crystalline layer properties, specifically strong in-plane but weak out-of-plane intermolecular interactions, which made it possible to exfoliate molecular sheets from the bulk 2D crystalline layers along the out-of-plane direction (direction a). The exfoliated thin 2D crystalline sheets could be used as an attractive platform for the construction of ultrathin *n*-type SC-OFETs. To test this possibility, we tried to exfoliate molecular layers from the **B**-phase 2D crystalline layer films via the "mechanical cleavage method", using cellophane tape; this imitates the early stage technique for obtaining graphene from graphite[16,17] (details in Experimental Section, Figure 5c). It was found that 2−10 monolayers (ca. 3−15 nm thickness) of CN-TFPA with neat terrace structures were stripped and successfully transferred onto the target SiO_2/Si substrates, binding tightly in the plane ***bc*** to maintain a large sheet area (ca. 100−200 μm) (Figure 5). The AFM image and surface profile in Figure 6a show that the CN-TFPA terrace films transferred onto the SiO_2/Si substrates

dx.doi.org/10.1021/cm301775c | Chem. Mater. 2012, 24, 3263−3268

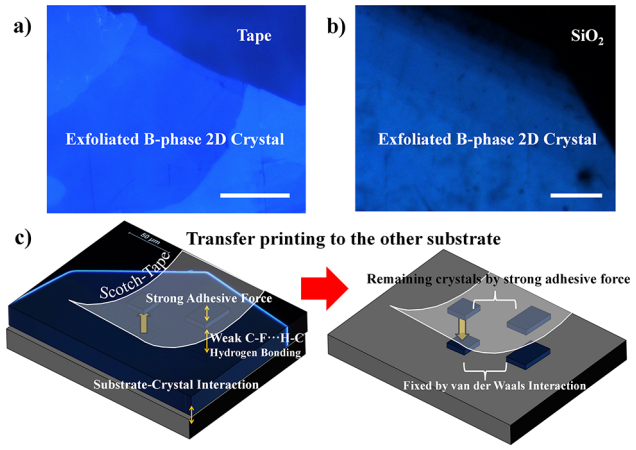

Figure 5. Fluorescent images of exfoliated **B**-phase 2D crystal on Scotch tape (scale bar: 30 μm) (a) and on SiO_2 substrate after the retransfer process (scale bar: 20 μm) (b). Schematic illustration of the mechanical cleavage method (c).

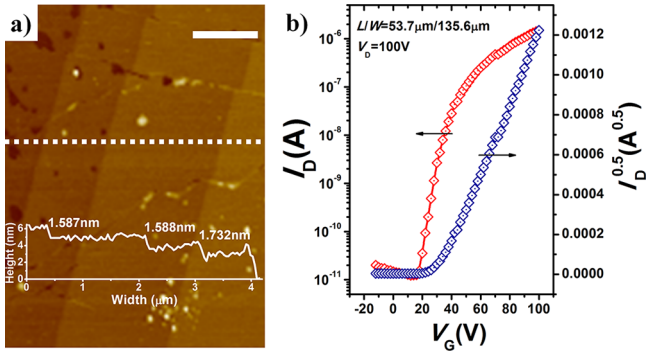

Figure 6. AFM image (scale bar: 1 μm) of an exfoliated **B**-phase 2D crystal on a SiO_2 substrate (inset: thickness profile along dashed white line) (a). Measured *n*-type transfer characteristics of the exfoliated **B**-phase 2D crystal (b).

were of good quality, and had the same terrace height (1.64 nm) as the mother **B**-phase 2D crystalline films (1.60 nm, d_{100}: 1.63 nm). Top-contact OFETs based on these exfoliation-transferred crystalline layer films—and their mother crystals—were successfully fabricated, and their transistor properties were investigated. Figure 6b shows that the OFETs based on these exfoliated 2D crystalline layers with a thickness of ~30 nm exhibited good *n*-type transistor behavior, with μ_e values of up to 0.053 $cm^2\ V^{-1}\ s^{-1}$; their mother crystals exhibited μ_e values of up to 0.30 $cm^2\ V^{-1}\ s^{-1}$ (Supporting Information, Figure S8), which were comparable to the value shown by the intact **B**-phase 2D crystalline film. We believe that the lower μ_e values (compared with the OFETs based on the **B**-phase 2D crystalline layer films, for which μ_e = 0.55 $cm^2\ V^{-1}\ s^{-1}$) resulted from physical contact problems occurring during the retransfer procedures. Further experimental investigation is required to estimate the effects of changes in the thickness of the active organic semiconducting layers on μ_e. Nevertheless, the uniform 2D crystal formability and exfoliation capability of the material with moderate *n*-type charge carrier transporting characteristic suggest great potential for flexible electronics application. By combining mechanical cleavage methods with a crystal patterning technique based on surface treatment,[18] we believe repetitive formation of ultrathin crystal patterns will be practicable which is suitable for flexible SC-OFETs with reasonable throughput device processing.

CONCLUSIONS

In conclusion, we report herein that CN-TFPA molecules acting as building blocks for high-performance *n*-type SC-OFETs showed a strong tendency to self-assemble into highly ordered 2D crystalline terrace structures with lowered LUMO levels; these structures are denoted here as **G**-phase and **B**-phase layers. These layers were deposited on substrates over a large area via a simple solution process that exploited the unique CF3-substituted DCS molecular system. The SC-OFETs of the **B**-phase CN-TFPA 2D crystalline layer films showed electron mobilities (μ_e) of up to 0.55 $cm^2\ V^{-1}\ s^{1-}$. Small numbers (2−10) of CN-TFPA monolayers with neat terrace structures could be exfoliated and transferred onto the target substrates using a simple "mechanical cleavage" method. The top-contact OFETs based on the exfoliated CN-TFPA 2D ultrathin crystalline layers (which had thicknesses of ~30 nm) also exhibited excellent *n*-type transistor behavior.

ASSOCIATED CONTENT

Supporting Information

Crystallographic information, schematic illustration of experimental methods, UV−visible spectra, PL spectra and optical microscope images of OFETs, crystallographic data (CCDC 885399). This material is available free of charge via the Internet at http://pubs.acs.org. CCDC 885399 contains the supplementary crystallographic data for this paper. These data can be obtained free of charge via www.ccdc.cam.ac.uk/data_request/cif, or by emailing data_request@ccdc.cam.ac.uk, or by contacting The Cambridge Crystallographic Data Centre, 12, Union Road, Cambridge CB2 1EZ, UK; fax: +44 1223 336033.

AUTHOR INFORMATION

Corresponding Author

*E-mail: parksy@snu.ac.kr.

Notes

The authors declare no competing financial interest.

ACKNOWLEDGMENTS

This research was supported by Basic Science Research Program (CRI; RIAMI-AM0209(0417-20090011)) and WCU (World Class University) project (R31-2008-000-10075-0) through National Research Foundation of Korea funded by the Ministry of Education, Science and Technology.

REFERENCES

(1) (a) Li, R.; Hu, W.; Liu, Y.; Zhu, D. *Acc. Chem. Res.* **2010**, *43*, 529. (b) Sundar, V. C.; Zaumseil, J.; Podzorov, V.; Menard, E.; Willett, R. L.; Someya, T.; Gershenson, M. E.; Rogers, J. A. *Science* **2004**, *303*, 1644. (c) Jiang, L.; Dong, H.; Hu, W. *J. Mater. Chem.* **2010**, *20*, 4994.

(2) (a) Jiang, L.; Dong, H.; Meng, Q.; Li, H.; He, M.; Wei, Z.; He, Y.; Hu, W. *Adv. Mater.* **2011**, *23*, 2059. (b) Wu, Q.; Li, R.; Hong, W.; Li, H.; Gao, X.; Zhu, D. *Chem. Mater.* **2011**, *23*, 3138.

(3) (a) Minemawari, H.; Yamada, T.; Matsui, H.; Tsutsumi, J.; Haas, S.; Chiba, R.; Kumai, R.; Hasegawa, T. *Nature* **2011**, *475*, 364. (b) Nakayama, K.; Hirose, Y.; Soeda, J.; Yoshizumi, M.; Uemura, T.; Uno, M.; Li, W.; Kang, M. J.; Yamagishi, M.; Okada, Y.; Miyazaki, E.; Nakazawa, Y.; Nakao, A.; Takimiya, K.; Takeya, J. *Adv. Mater.* **2011**, *23*, 1626.

(4) Gsänger, M.; Oh, J. H.; Könemann, M.; Höffken, H. W.; Krause, A.-M.; Bao, Z.; Würthner, F. *Angew. Chem., Int. Ed.* **2010**, *49*, 740.

(5) Oh, J. H.; Suraru, S.-L.; Lee, W.-Y.; Könemann, M.; Höffken, H. W.; Röger, C.; Schmidt, R.; Chung, Y.; Chen, W.-C.; Würthner, F.; Bao, Z. *Adv. Funct. Mater.* **2010**, *20*, 2148.
(6) Yoon, M.-H.; Facchetti, A.; Stern, C. E.; Marks, T. J. *J. Am. Chem. Soc.* **2006**, *128*, 5792.
(7) Shoji, K.; Nishida, J.-I.; Kumaki, D.; Tokito, S.; Yamashita, Y. *J. Mater. Chem.* **2010**, *20*, 6472.
(8) Yun, S. W.; Kim, J. H.; Shin, S.; Yang, H.; An, B.-K.; Yang, L.; Park, S. Y. *Adv. Mater.* **2012**, *24*, 911.
(9) Kim, J. H.; Chung, J. W.; Jung, Y.; Yoon, S. J.; An, B.-K.; Huh, H. S.; Lee, O. W.; Park, S. Y. *J. Mater. Chem.* **2010**, *20*, 10103.
(10) (a) An, B.-K.; Kwon, S.-K.; Jung, S.-D.; Park, S. Y. *J. Am. Chem. Soc.* **2002**, *124*, 14410. (b) An, B.-K.; Lee, D.-S.; Lee, J.-S.; Park, Y.-S.; Song, H.-S.; Park, S. Y. *J. Am. Chem. Soc.* **2004**, *126*, 10232. (c) An, B.-K.; Gierschner, J.; Park, S. Y. *Acc. Chem. Res.* **2012**, *45*, 544.
(11) Ando, S.; Murakami, R.; Nishida, J.-I.; Tada, H.; Inoue, Y.; Tokito, S.; Yamashita, Y. *J. Am. Chem. Soc.* **2005**, *127*, 14996.
(12) Yamao, T.; Miki, T.; Akagami, H.; Nishimoto, Y.; Ota, S.; Hotta, S. *Chem. Mater.* **2007**, *19*, 3748.
(13) (a) Hunter, C. A. *Angew. Chem., Int. Ed.* **1993**, *32*, 1584. (b) Cozzi, F.; Cinquini, M.; Annuziata, R.; Siegel, J. S. *J. Am. Chem. Soc.* **1993**, *115*, 5330.
(14) Desiraju, G. R. *Acc. Chem. Res.* **2002**, *35*, 565.
(15) (a) Weissbuch, I.; Addadi, L.; Leiserowitz, L. *Science* **1991**, *253*, 637. (b) Barbarella, G.; Zambianchi, M.; Antolini, L.; Ostoja, P.; Maccagnani, P.; Bongini, A.; Marseglia, E. A.; Tedesco, E.; Gigli, G.; Cingolani, R. *J. Am. Chem. Soc.* **1999**, *121*, 8920.
(16) Novoselov, K. S.; Geim, A. K.; Morozov, S. V.; Jiang, D.; Zhang, Y.; Dubonos, S. V.; Grigorieva, I. V.; Firsov, A. A. *Science* **2004**, *306*, 666.
(17) Jiang, H.; Tan, K. J.; Zhang, K. K.; Chen, X.; Kloc, C. *J. Mater. Chem.* **2011**, *21*, 4771.
(18) (a) Briseno, A. L.; Mannsfeld, S. C. B.; Ling, M. M.; Liu, S.; Tseng, R. J.; Reese, C.; Roberts, M. E.; Yang, Y.; Wudl, F.; Bao, Z. *Nature* **2006**, *444*, 913. (b) Briseno, A. L.; Aizenberg, J.; Han, Y.-J.; Penkala, R. A.; Moon, H.; Lovinger, A. J.; Kloc, C.; Bao, Z. *J. Am. Chem. Soc.* **2005**, *127*, 12164.